ACS AuthorChoice

Terms of Use

ARTICLE

Tunable Adsorption of Soft Colloids on Model Biomembranes

Adriana M. Mihut, Aleksandra P. Dabkowska,* Jérôme J. Crassous,* Peter Schurtenberger, and Tommy Nylander

Physical Chemistry, Department of Chemistry, Lund University, 22100 Lund, Sweden

ABSTRACT A simple procedure is developed to probe *in situ* the association between lipid bilayers and colloidal particles. Here, a one-step method is applied to generate giant unilamellar 1,2-dioleoyl-*sn*-glycero-3-phosphocholine (DOPC) vesicles (GUVs) by application of an alternating electric field directly in the presence of thermoresponsive poly(*N*-isopropylacrylamide) (PNIPAM) microgels. We demonstrate that the soft PNIPAM microgel particles act as switchable stabilizers for lipid membranes. The change of the particle conformation from the swollen to the collapsed state enables the reversible control of the microgel adsorption as a function of temperature. At 20 °C, the swollen and hydrophilic soft microgel particles adsorb evenly and densely pack in 2D hexagonal arrays at the DOPC GUV surfaces. In contrast, at 40 °C, that is, above the volume phase transition temperature (T_{VPT} = 32 °C) of the PNIPAM microgels, the collapsed and more hydrophobic particles partially desorb and self-organize into domains at the GUV/GUV interfaces. This study shows that thermoresponsive PNIPAM microgels can be used to increase and control the stability of lipid vesicles where the softness and deformability of these types of particles play a major role. The observed self-assembly, where the organization and position of the particles on the GUV surface can be controlled "on demand", opens new routes for the design of nanostructured materials.

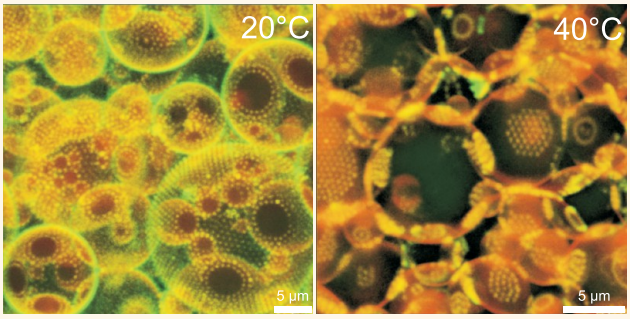

KEYWORDS: giant unilamellar vesicles · lipid membranes · DOPC lipid bilayer · PNIPAM microgel particles

Cellular membranes are self-assembled structures that not only compartmentalize and protect the cell but also harbor the biomolecules necessary for many key biological processes. To make use of these membrane-coupled interactions in nanotechnology, model membranes can be used either to mimic nature or to tune their physicochemical properties to specific technological applications.[1−9] Giant unilamellar vesicles (GUVs) consist of a single phospholipid bilayer that encloses a spherical aqueous compartment of the same size as that of common cells (1−100 μm). The lipid bilayer is the simplest mimic of the biological membrane barrier function and also mimics the fluidity of the lipid matrix incorporating membrane proteins. Therefore, GUVs are often used for studying biological processes at the lipid membrane, as reviewed by Walde *et al.*[10] Beyond the use of GUVs to study the physical properties of membranes[11,12] and biomolecular interactions,[13] there is wide interest in using GUVs as biosensors, nanoreactors,[14] and miniature compartments for synthetic biology.[15] In order to extend the capabilities of these latter applications, the integration of GUVs with already-existing smart materials is of paramount importance.

Decorating lipid vesicles with polymers is commonly done to improve their drug delivery capability,[16] including increasing their stability[17−19] and biocompatibility.[20] Thermoresponsive and pH-responsive polymers that feature a volume phase transition[21] exhibit great potential for the development of smart composite materials[22,23] and as building blocks for complex self-assembly from their ability to adapt both their conformation and interaction potential to their local environment.[24−28] Microgel particles (*i.e.*, cross-linked polymer particles that are swollen by a solvent) have been recently identified as a new class of responsive stabilizers of emulsions or so-called pickering agents at oil/water interfaces.[29−35] Moreover, on one hand, it is anticipated that such hydrogel particles used as templates for the adsorption of a lipid bilayer to form

* Address correspondence to aleksandra.dabkowska@fkem1.lu.se, jerome.crassous@fkem1.lu.se.

Received for review July 26, 2013 and accepted November 5, 2013.

Published online November 05, 2013
10.1021/nn403892f

© 2013 American Chemical Society

lipogels[36] will prove to be useful in drug delivery, tissue engineering applications, and in fundamental biophysical studies of membranes.[36−38] On the other hand, it has already been reported that polymer-gel-containing giant vesicles can be prepared through the UV light-induced polymerization of liposome-encapsulated hydrophilic monomers, by the encapsulation of a cross-linked copolymer network to the inner monolayer or by direct pressure microinjection into the GUVs.[39−43] Furthermore, when used as substrate, microgels have shown great potential in cell culture engineering where the particle films can be used as switchable cell substrates to control the detachment of adsorbed cells by changing the temperature.[44]

Understanding how nanoparticles interact with lipid bilayers will potentially have a high impact on the development of new drug delivery systems and on the investigation of their cytotoxicity. A growing number of simulation and experimental studies have revealed the effect of the chemical nature, surface functionalization, and size on the interaction with lipid bilayers.[45−51] These studies have more recently involved the effect of the shape,[52−60] which is more complex as it also depends on the size and surface chemistry of the particles. To gain further fundamental knowledge to apply these systems, new methods and experiments with model colloidal systems are required. If nanoparticles could be designed to change shape once they reach the biomembrane, the delivery efficiency could be improved and controlled. Nevertheless, to the best of our knowledge, while the lipid adsorption at the surface of hydrogel particles where the particles were used as solid supports has been recently reported,[36,38,61,62] there is still no systematic study on soft nanoparticle adsorption to model lipid membranes. In this study, we investigate soft microgel particles that can serve as a simple proxy to biological soft colloidal entities, like protein assemblies, cells, or cell organelles in biological systems. The advantage of the used particles is that they exhibit a rapid phase transition close to human body temperature, which affects the softness, hydrophobicity, and size of the nanoparticles and in turn affects the interactions with the lipid bilayer.

We describe a one-step procedure to obtain a hybrid composite consisting of giant 1,2-dioleoyl-*sn*-glycero-3-phosphocholine (DOPC) unilamellar vesicles (GUVs) generated by an electric field and decorated with spherical PNIPAM microgel particles. This novel method significantly reduces preparation time and allows for a wider choice of materials and a better control over the resulting morphology. The hybrid system can be controlled as a function of temperature as the microgel particles exhibit a reversible volume phase transition in water around 32 °C. Below the phase transition, the particles significantly stabilize the vesicles. We show that, above the volume phase transition temperature T_{VPT}, the lipid bilayer/microgel interaction is altered in such a way that the microgels rearrange into domains at the vesicle interface that significantly reduces the particle stabilization.

RESULTS AND DISCUSSION

Microgel Characterization. The microgels employed in this study were prepared by surfactant-free emulsion polymerization of *N*-isopropylacrylamide (NIPAM) with *N*,*N*′-methylenebis(acrylamide) (BIS) as cross-linker (5 mol % cross-linking) and employing 2,2′-azobis-(2-methylpropionamidine)dihydrochloride (V50) as the initiator. In addition, the particles were noncovalently stained by adding a water-soluble fluorescein dye. The microgels are well-defined and monodisperse as confirmed by the statistical analysis of the TEM micrographs using a population of more than 100 isolated particles. The average diameter determined in the dried state was found equal to 632 ± 82 nm (Figure 1A). Similar values were obtained from the SFM height images where the microgel average diameter was determined at 835 ± 45 nm and the film height at 113 ± 3 nm (Figure 1B). The SFM results confirm that these particles are soft, as they spread at the surface and adopt a so-called "fried egg" configuration as reported previously.[44,63] The differences in particle sizes revealed by TEM and SFM arise from the different strength of the forces between the particles and the carbon grid and the silicon substrates used in the two techniques, respectively. In comparison, dynamic light scattering (DLS) was employed to estimate the temperature dependence of the hydrodynamic radius R_H of the particles in suspension. In the so-called "swollen" state at 20 °C, R_H is equal to 443 nm and then continuously decreases to 347 nm at 30 °C, close to the volume transition temperature T_{VPT} = 32 °C as expected for PNIPAM microgels. Above T_{VPT}, at 35 °C, the PNIPAM network collapses and R_H remains constant at a value of about 256 nm. This transition was directly imaged using confocal laser scanning microscopy (CLSM), as shown in Figure 1C,D. The transition from swollen to collapsed is clearly visible for the fluorescent particles adsorbed at the surface of the cover glass slide, and we can qualitatively compare the sizes from the images to the hydrodynamic radius R_H determined by DLS (dashed circles in Figure 1C,D). Even if the microgel particles were synthesized without any addition of surfactant, they still bear some positive charges due to the amidine end groups arising from the V50 initiator. The presence of the cationic charges was confirmed by a slightly positive ζ-potential value measured of 2 mV at 20 °C. The ζ-potential continuously increases with the temperature to a value of about 12 mV at 50 °C, and with a transition around 32 °C that coincides with the decrease of R_H. These results reflect both the low surface charge density and the high frictional coefficient at low temperature and the transition to a collapsed state with higher charge density and lower frictional coefficient.[64]

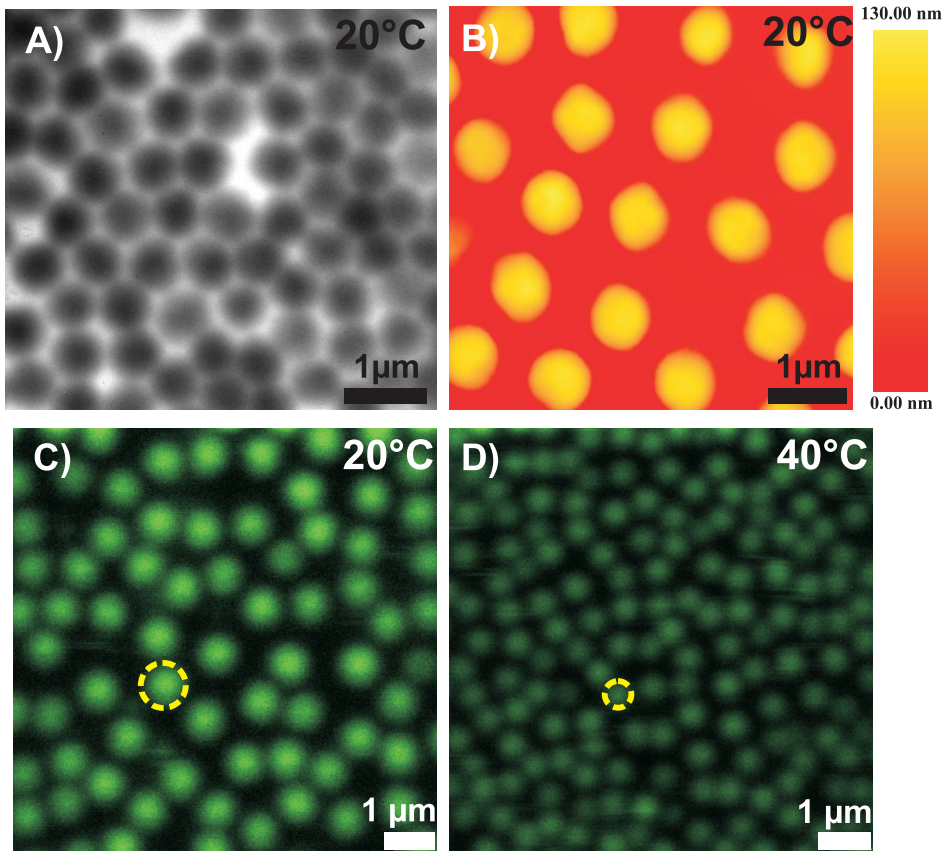

Figure 1. (A) TEM micrograph and (B) SFM height image of the PNIPAM microgels in air on carbon-coated copper grid and silicon wafer, respectively. PNIPAM microgels were imaged at the water/glass interface by CLSM at 20 °C (C) and 40 °C (D). The dashed circles around the entire particles give the hydrodynamic radii R_H determined in the swollen and collapsed state by DLS.

The microgel structure was further investigated using small-angle X-ray scattering (SAXS). Dilute non-interacting suspensions were measured at 20 and 40 °C. Our analysis follows the procedure of Stieger *et al.*[65] For centro-symmetric particles, the scattering intensity $I(q)$ is

$$I(q) = \frac{N}{V}\Delta\rho_e^2 V_p^2 P(q)S(q) \quad (1)$$

where N/V refers to the particle number density, $\Delta\rho_e$ is the difference of contrast length density between PNIPAM and water, and V_p is the volume of PNIPAM in a particle. The form factor $P(q)$ describes the scattering of a single particle, and the structure factor $S(q)$ accounts for interparticle correlations due to interaction effects. At sufficiently low concentration, the influence of $S(q)$ on the scattering intensity can be disregarded. Hence, in our analysis, we can assume that $S(q) = 1$. In the case of microgel particles, $P(q)$ can be decomposed into two terms:

$$P(q) = I_{part}(q) + I_{fluc}(q) \quad (2)$$

$I_{part}(q)$ is the part of $P(q)$ related to the average electronic density profile of the particles, and $I_{fluc}(q)$ refers to the contributions from the thermal fluctuation of the PNIPAM network. Hereby, static inhomogeneities and thermal fluctuations within the polymeric network can be described in the form of a Lorentzian function as

$$I_{fluc}(q) = \frac{I_{fluc}(0)}{1 + \xi^2 q^2} \quad (3)$$

where ξ refers to the average correlation length and $I_{fluc}(0)$ is an adjustable parameter. Note that $I_{fluc}(q)$ contributes significantly only in the high q regime. In our analysis, the scattering intensity is only considered in arbitrary units, and therefore, $\Delta\rho_e$ and N/V can be treated as adjustable parameters in the following analysis. At room temperature, the density profile of PNIPAM microgels is not homogeneous but rather decays as an error function. This is a direct consequence of the difference of reactivity between the monomer and the cross-linker.[66] Such structure is described with the following functional form:

$$P(q) = \left[\frac{3[\sin(qR) - qR\cos(qR)]}{(qR)^3}\exp\left(-\frac{\sigma^2 q^2}{2}\right)\right]^2 + I_{fluc}(q) \quad (4)$$

R is the half-width radius, where the scattering length density is half of the core density, and 2σ is the half-width of the shell. The total radius determined from this analysis is $R_{SAXS} = R + 2\sigma$, and the size of the core

defined by a constant polymer volume fraction ϕ_c is $R_c = R - 2\sigma$. Such formalism results in the following expression for the normalized radial polymer volume fraction profile $\phi(r)/\phi_c$:

$$\frac{\phi(r)}{\phi_c} = \begin{cases} 1: & r \le R_c \\ 1 - (R - r - 2\sigma)^2/(8\sigma^2): & R_c < r \le R \\ (r - R - 2\sigma)^2/(8\sigma^2): & R < r < R_{SAXS} \\ 0: & R_{SAXS} \le r \end{cases} \quad (5)$$

Such description is valid for monodisperse particles. Nevertheless, the microgels investigated may be polydisperse, which was considered by assuming a Gaussian distribution of the particle radius:

$$D(R, \langle R \rangle, \sigma_{poly}) = \frac{1}{\sqrt{2\pi\sigma_{poly}^2\langle R \rangle^2}} \exp\left(-\frac{(R - \langle R \rangle)^2}{2\sigma_{poly}^2\langle R \rangle^2}\right) \quad (6)$$

with $\langle R \rangle$ referring to the average particle radius and σ_{poly} denoting the relative size polydispersity. Therefore, for noninteraction particles, the scattering intensity can be expressed as follows:

$$I(q) = \frac{N}{V}\Delta\rho_e^2 \int_0^\infty D(R, \langle R \rangle, \sigma_{poly}) V_p(R)^2 P(q, R) dR \quad (7)$$

This model provides a reasonably good description of the data presented in Figure 2B and asserts the conformational transformation occurring with the temperature. The data have been fitted from 4×10^{-3} to 0.5 nm^{-1}. At 20 °C, the particles are fuzzy with R determined at 341.9 ± 6.7 nm and σ = 34.2 ± 2.5 nm. This procedure leads to an overall size determined by SAXS of 410.3 ± 11.7 nm with 6.5 ± 1.6% relative polydispersity, in good agreement with the hydrodynamic radius of the particle, which is about 33 nm larger. We see clear deviations at $q > 0.04$ nm^{-1} related to the internal structure of the particles. The reason for these deviations is linked to the contrast situation encountered in X-ray scattering experiments with core−shell structures. These higher-order oscillations are extremely sensitive to the delicate balance and exact details of the radial excess scattering length density profile, the background and the fluctuation term, where minor variations in a specific parameter result in significant variations of the high q oscillations in $I(q)$. Given the fact that the purpose of this article is not an in-depth refinement of the currently used models for the analysis of the SAXS data for microgels, but rather to present experimental evidence of the volume phase transition including the dramatic change of their size and fuzziness at higher temperature, we refrain from a further refinement of the local structure of the fuzzy shell. At 40 °C, the microgel network collapses and the loss of the fuzzy shell structure results in a much more regular SAXS pattern with well-defined minima and maxima that are well

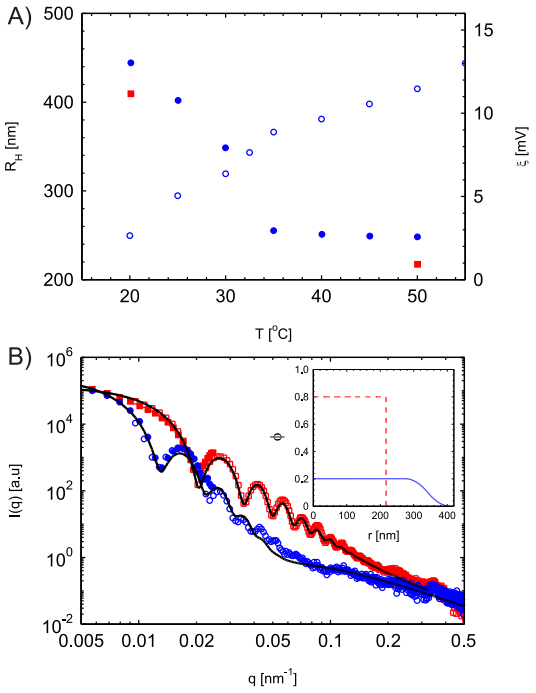

Figure 2. (A) Hydrodynamic radius of PNIPAM microgel as determined by DLS (filled blue circles) and variation of the ζ-potential (open empty circles) in dependence of the temperature. The red filled squares represent the overall microgel size determined by SAXS at 20 and 40 °C. (B) SAXS scattering intensities of PNIPAM microgel at 20 °C (empty blue circles) and 40 °C (empty red squares). Variation of the scattering intensity of the PNIPAM microgel as determined by SLS at 20 °C (filled blue circles) and 40 °C (filled red squares). The inset shows the corresponding density profiles at 20 °C (filled blue line) and 40 °C (dashed red line).

captured by the simple homogeneous sphere model with a radius of 217.4 ± 2.5 nm. The polydispersity decreases to 4.5 ± 1% as the particles become more defined. This transition is also visible in the local network structure as ξ varies from 10.5 ± 1.7 to 7.1 ± 3.2 nm. The corresponding polymer density profiles are presented in the inset of Figure 2B. Even in their collapsed state, PNIPAM microgels still contain about 20−30 wt % water.[65,67] Therefore, in our analysis, we assume that ϕ_c = 0.8 at 40 °C. Doing so and maintaining the total mass constant, we found ϕ_c to be around 0.2 in the swollen state at 20 °C.

***In Situ* Study of PNIPAM Microgel Adsorption to Supported Lipid DOPC Bilayers.** Microgel particle adsorption onto solid-supported lipid bilayers was monitored *versus* time in a liquid flow cell *via* QCM-D. DOPC bilayers were formed on the SiO_2 surface of QCM-D sensors *via* the vesicle fusion technique (see Figure S1 in Supporting Information).[68] The mass (m) of the lipids deposited on the surface was assessed using the Sauerbrey equation:

$$\Delta m = \frac{c}{n}\Delta F \quad (8)$$

where c is the Sauerbrey constant (17.7 ng cm^{-2}), ΔF is the frequency shift, and n is the overtone number.

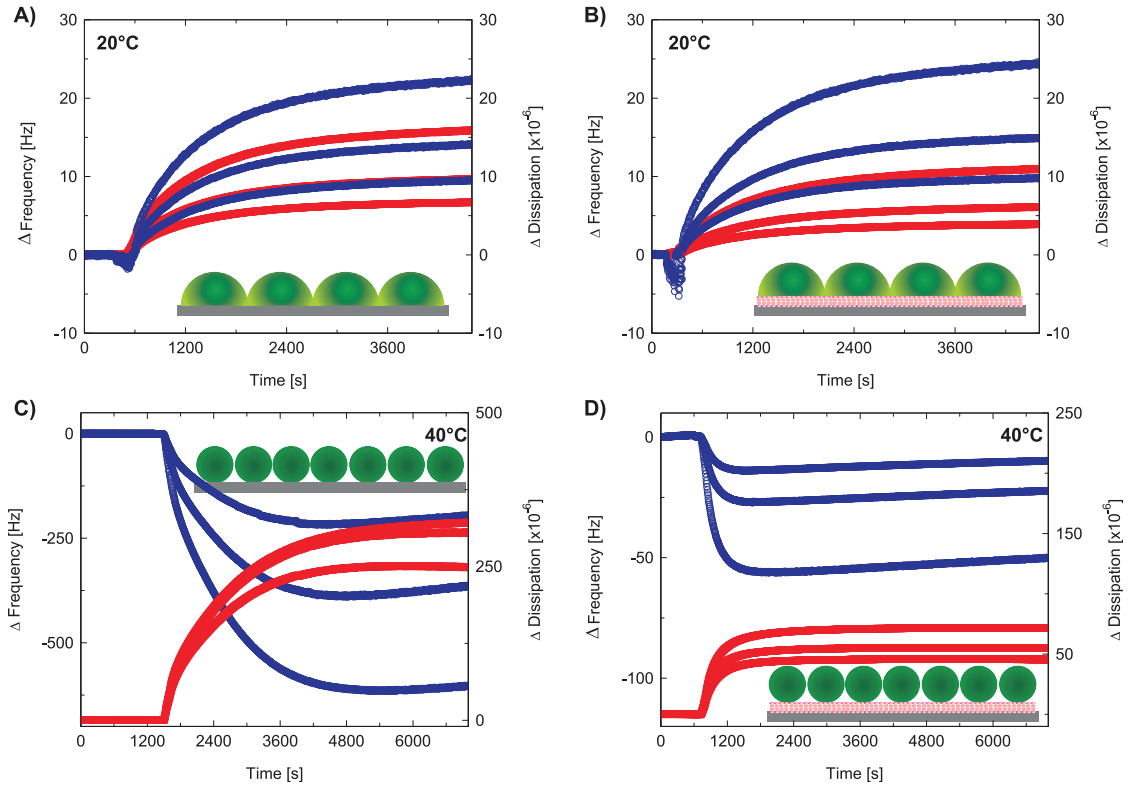

Figure 3. QCM data for (A) bare microgels and (B) bilayer with microgels at 20 °C, (C) bare microgels and (D) bilayer with microgels at 40 °C. The blue open circles represent the resonance frequency *vs* time measurements, whereas the red squares represent the dissipation *vs* time measurements. Schematic representation of the particle adopted conformation after adsorption on the SiO_2 substrate and on the lipid bilayer at 20 and 40 °C, that is, when the particles are soft and hard, respectively. Gray, SiO_2 substrate; green, PNIPAM microgel particles; pink, lipid bilayer.

The Sauerbrey equation has been shown to adequately describe compact films[69] including lipid bilayers.[70] In this case, the mass calculated from the seventh harmonic was found to be 410 to 430 ng cm^{-2}, consistent with a high DOPC bilayer coverage of the surface. This results in an area per DOPC molecule of 0.64 nm^2 comparable to previously reported studies using QCM-D or X-ray and neutron diffraction experiments.[70−72] Subsequently, the PNIPAM microgel dispersion (0.14 wt %) was injected into the QCM-D cells, either onto the adsorbed phospholipid bilayers or onto bare SiO_2 substrate. Measured changes in frequency (ΔF) and dissipation (ΔD) are presented in Figure 3 and Figure 4. Since rinsing with water resulted in very little change in ΔF and ΔD, the adhesion to the surface appears to be irreversible on all surfaces.

At the low temperature (20 °C), injection of the microgel onto the bilayer resulted in an increase in both frequency and dissipation (Figure 3B). Such positive changes in frequency shift are expected when large particles weakly attach to a surface[73] and have been observed for the soft adhesion of bacterial cells to surfaces,[74,75] as well as the adsorption of submicrometer TiO_2 particles to silica.[76] Control measurements obtained on a bare SiO_2 surface without preadsorbed bilayers also displayed positive ΔF and ΔD (Figure 3A). The extensive attachment of the microgels to the SiO_2 surface was also observed using fluorescence (Figure 1), and the driving force for the particle attachment is likely to be electrostatic in nature. The positive shifts in ΔF are similar in amplitude for the bilayer and the bare

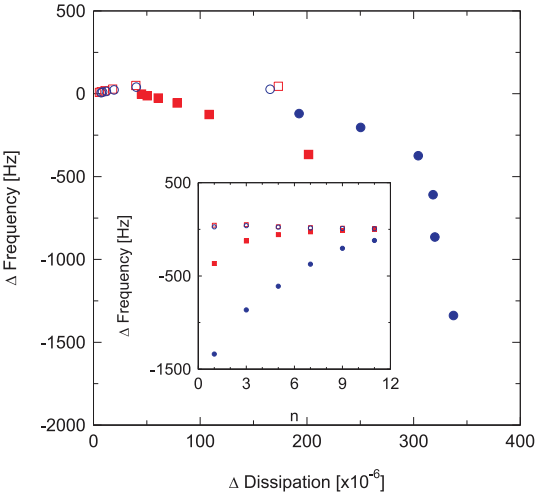

Figure 4. Change in resonance frequency *vs* change in dissipation for all overtones at 20 °C (the blue open circles correspond to bare microgel, and the red open squares correspond to the bilayer with microgel) and at 40 °C (the blue filled circles correspond to bare microgel, and the red filled squares correspond to the bilayer with microgel). The inset shows the change in resonance frequency *versus* the overtone number.

TABLE 1. Relative Changes in Frequency ΔF, Dissipation ΔD, and Ratios $\Delta D/\Delta F$ after Adsorption of Microgel Particles to Bare Silicon Oxide or Supported Bilayer after Rinsing Calculated from the Seventh Overtone

conditions	ΔF (Hz)	ΔD ($\times 10^{-6}$)	$\Delta D/\Delta F$ ($\times 10^{-6}$ s)
20 °C microgel	14.59 ± 0.04	11.99 ± 0.02	0.82
20 °C bilayer + microgel	15.16 ± 0.11	6.12 ± 0.04	0.40
40 °C microgel	−384.16 ± 3.20	300.38 ± 2.52	−0.78
40 °C bilayer + microgel	−22.48 ± 0.34	55.15 ± 0.05	−2.45

SiO_2, but the ΔD increase is about twice as high for the microgels on the bare surface. This suggests a reduction of the lateral dissipation modes when the microgel particles are adsorbed onto the fluid bilayer.[77]

When the temperature was increased to 40 °C, a completely different adsorption behavior was observed. The addition of the microgels resulted in a negative shift in ΔF and a positive shift in ΔD on both the bilayer and the bare SiO_2 surface (Figure 3C,D). However, the frequency shift in the presence of a bilayer is nearly 17 times lower (−22.48 ± 0.34 Hz *vs* −384.16 ± 3.20 Hz for the bare silicon compared at the seventh overtone). The ΔD is more than 5 times lower on the bilayer. Thus, it appears that the bilayer is shielding the surface−microgel interaction and screening the electrostatic attractive interaction between the negative SiO_2 surface and the positive charged microgels. Under these conditions, the response of the resonator is nonlinear for the overtones with both ΔF and ΔD splitting for the overtones (Figure 4). The changes in dissipation after the PNIPAM microgel adsorption and rinsing at different temperatures are summarized in Table 1.

These results show two distinct scenarios of microgel adsorption on the DOPC bilayers depending on the adopted shell conformation of the microgel particles at different temperatures. When the adsorption occurs at 20 °C, the particles may spread and cover most of the surface. This "fried egg" configuration maximizes the contact area between the microgels and the DOPC bilayer, giving rise to a more homogeneous interface. On the other hand, at 40 °C, the collapsed microgel particle conformation and the resulting strong interparticle interactions are expected to lead to the development of a more inhomogeneous adsorbed layer. As the microgel shell collapses and the particles become smaller and much less deformable, the surface contact area between the microgels and the lipid bilayer becomes reduced. However, at both temperatures, the large dissipation caused by the viscoelasticity of the adsorbed layer puts the data outside of the Sauerbrey analysis regime, which requires that the layers are thin and rigid. The Voigt viscoelastic model, which has been successfully used to determine thickness, shear modulus, and viscosity of surface layers, requires soft and laterally homogeneous films.[69] In this case, the solvent contribution to the QCM-D signal depends on a series of specific parameters such as surface coverage, orientation, and surface attachment of the particles.[78] Recently, Reviakine *et al.* reviewed the limitations of current QCM-D theory and also the promising headway that researchers are making in finding appropriate models to analyze more complex surface structures.[77] It is clear that QCM-D is a very sensitive technique that catches the two distinct temperature-dependent adsorption behaviors of the microgel particles on the lipid bilayer. Nevertheless, the quantitative interpretation of the data is still limited by the existing models which cannot be directly applied to evaluate the adsorption of discrete and relatively large particles forming heterogeneous thick films, as those used in the present study.

To support the qualitative assessment of the particle adsorption based on the results from the QCM-D, the adsorption of microgel particles from an aqueous dispersion to the phospholipid bilayers was also followed *in situ* with ellipsometry at 25 and 40 °C as described in detail in the Experimental Section. As for the previous experiments, prior to the microgel adsorption, the phospholipid bilayer with a characteristic thickness of 4.5 nm was formed. The film thickness changed significantly after the microgel addition, indicating the adsorption of microgels to the phospholipid layer. The adsorbed microgel film thickness was not affected by extensive rinsing, demonstrating that the particles are strongly attached to the bilayer surface. The calculated microgel film thickness in dispersion at 25 °C was found to be 301 nm, whereas at 40 °C, it was 230 nm. A thickness of 4.1 nm was determined for the phospholipid bilayer at 40 °C. The ellipsometry data revealed that the average film thickness is about twice that of the dried microgel particles measured by SFM. However, it is only half of the film thickness expected from adsorption of intact particles, based on the hydrodynamic radius in dispersion. This implies flattening of the particles upon adsorption on the silicon surface. A similar behavior has previously been reported for fuzzy PNIPAM-*co*-poly(acrylic acid) microgel particles where the dried microgel was investigated by SFM. The average height of the dried particle film was found to be 10 times lower than the apparent hydrodynamic diameter of the particles measured by light scattering.[63] A change of the effective refractive index, n_{eff}, was observed from 1.400 at 25 °C when the particles are swollen to 1.503 at 40 °C in the compact state from the fitting of our ellipsometry data. The refractive index and thickness changes reflect both the volume phase transition of the PNIPAM microgels shown by SAXS, as well as the number of particles adsorbed on the surface. The refractive index of the pure PNIPAM microgels, n_m, was determined at 25 °C by refractometry as 1.601. The corresponding measurement could not be performed at 40 °C as a consequence of the significant increase of the suspension

turbidity at high temperatures. Assuming that the refractive index and the density of the PNIPAM (ρ_{PNIPAM} = 1.1492 g cm^{-1}) are not significantly affected by the temperature, we could estimate the average polymer volume fraction of the adsorbed layer, ϕ_l, as $n_{eff} = n_m\phi_l + n_w(1 - \phi_l)$, where n_w is the refractive index of water; ϕ_l was found equal to 0.222 and 0.610 at 25 and 40 °C, respectively. These values are in reasonable agreement with the SAXS analysis and refer to a variation of the adsorbed mass, $m = \phi_l/\rho_{PNIPAM}$ from 7684 to 16 114 ng cm^{-2} with increasing temperature. If we now consider the average mass of a single microgel particle determined from the SAXS analysis in the collapsed state (see Figure 2B), we can evaluate the increase of the number of particles adsorbed per surface unit to 1.94 and 4.07 μm^{-2}. These values, compared to a close-packed monolayer determined as $0.9069/(\pi R_H(T)^2)$ at 1.73 and 4.50 μm^{-2} for the two temperatures, suggest a densely packed monolayer at both temperatures with an eventual interpenetration of the particles at 25 °C. In comparison, our confocal observations of the adsorption on a bare glass substrate reveal a similar increase of the surface coverage by a factor of about 2 from 1.16 μm^{-2} at 20 °C to 2.23 particles μm^{-2} at 40 °C with, however, about 2 times lower values (see Figure 1C,D).

Stabilization of GUVs with PNIPAM Microgels. Giant unilamellar vesicles were prepared *in situ* on indium tin oxide (ITO)-coated microscope coverslips using the electroformation method.[79] The lipid solution was deposited onto the conductive side of the ITO-coated glass and allowed to dry. Subsequently, the PNIPAM microgel dispersion was added onto the deposited lipid film before applying the electric field, which is expected to lead to immediate hydration of the lipid multilayer. The GUVs decorated with PNIPAM particles were prepared according to a one-step procedure at 20 °C, as schematically illustrated in Figure 5A. When an electric field of 6 V at a frequency of 50 Hz was applied to the lipid/water mixture, the GUVs formed instantaneously without including the microgel particles as observed directly with confocal fluorescence microscopy (see video in Supporting Information). The obtained GUVs display a very regular spherical shape with the radii in the range of several micrometers. After a few minutes, the microgel particles adsorbed on the GUV surface. No microgel particles were observed inside the GUVs. Figure 5B–D shows the corresponding confocal images of the GUV/microgel assemblies obtained in the dispersion a few minutes after the application of the electric field. The particles decorating the vesicles are evenly distributed and hexagonally pack as a monolayer on the surface of the GUVs (Figure 5B–D, 20 °C). An important observation is that decorated GUVs are significantly more stable (5 days) at ambient temperature in comparison with bare GUVs, which start to deform and fuse after a few hours, only. Interestingly, a careful examination of the 3D CLSM projection shows that no particles are present at the contact area between adjacent vesicles, as shown by the particle-free circular regions in Figure 5D. Given the hydrophilic nature of the particles at this temperature, we assume that they are attached to the lipid headgroup region and that the lateral mobility of the particles at the fluid bilayer interface is sufficiently high to squeeze them out from the vesicle/vesicle interface.

The use of microgel particles as stabilizers to fabricate oil-in-water emulsions is well-known. Schmitt *et al.* showed that, due to their softness, initially spherical PNIPAM microgels adopt a "fried egg-like" conformation when adsorbed at the oil/water interface.[33,34] The shape of the particles then becomes distorted on either side of the interface. This observation was supported by Geisel *et al.*, who reported that the outer corona of the microgel particles deforms and flattens along the contact line between particles, which led to the formation of a tightly packed honeycomb structure.[32] All these studies highlight the fundamental difference between soft microgels and rigid particles and the formers' enhanced efficiency as stabilizing agents. Since microgels can adapt their conformation to maximize the interfacial interactions, in both adsorption processes, either at oil–water interfaces or at the surface of the lipid membranes, the softness of the particles and their ability to laterally overlap promote their efficiency as stabilizers.

However, the situation changes drastically upon increasing the temperature above T_{VPT}. At 40 °C, the microgels partially desorb to rearrange into domains at the GUV/GUV interfaces (Figure 5E–G). A closer investigation of the GUV/microgel interface indicates an overlapping of the fluorescences. This suggests that the microgels perturb the vesicle bilayer and probably partly penetrate into the hydrophobic lipid acyl chain region. We however believe that they do not fully penetrate through the bilayers as the vesicles are intact. The self-organization into domains indicates an increase of the attractive particle–particle and particle–bilayer interactions. Consequently, the GUVs deform and facet. Nevertheless, no coalescence of the GUVs was observed during the measurements. The smaller and denser collapsed microgels are not sterically stabilized anymore and become more attractive due to the combined effect of the increased van der Waals and hydrophobic interactions. Indeed, PNIPAM microgels are known to aggregate above T_{VPT} in the absence of electrostatic interactions.[80] Such an aggregation process is partially or fully reversible with the temperature.[25,26] Similarly, in this study, we observe that the adsorption of the microgel particles on the GUVs is reversible when the system is brought back to 20 °C (data not shown here).

The different factors mentioned above are most probably at the origin of the particle rearrangement at

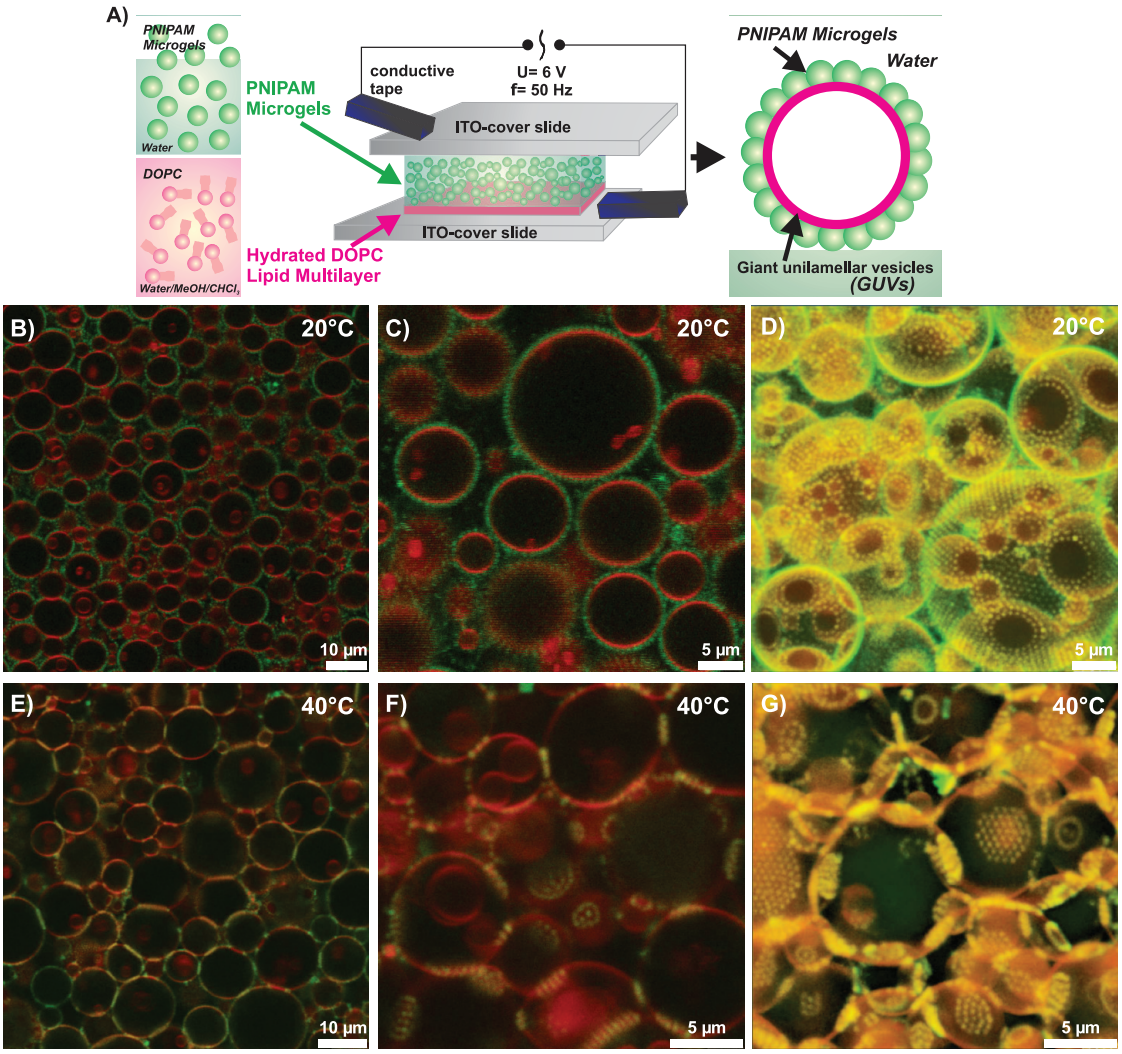

Figure 5. (A) Schematic description of the preparation of lipid giant vesicles (GUVs) in the presence of thermoresponsive PNIPAM microgels under the influence of an electric field at 20 °C. Fluorescence confocal micrographs of lipid giant vesicles decorated with the thermoresponsive PNIPAM microgels at 20 °C (B–D) and above the PNIPAM volume phase temperature transition V_{PTT} at 40 °C (E–G). Three-dimensional projection of the hybrid system which was reconstructed from confocal *z*-stack images at 20 °C (D) (42.12(*x*) × 42.12(*y*) × 20.9(*z*) μm^3) and at 40 °C (G) (36.06(*x*) × 36.06(*y*) × 17.04(*z*) μm^3).

the GUV interface. On the basis of these results, it can be inferred that the reduced lateral overlap of the particles along with the onset of attractive interactions gives rise to the coexistence of depleted zones with domains of hexagonally closed-packed particles. A similar observation was reported for pickering emulsions with microgel particles above T_{VPT}.[33,34] There, the authors observed that the stabilizing particle monolayer could be easily disrupted, causing the coalescence of the emulsion droplets. It is noteworthy that, in the current study, the microgels were found to adsorb on a solid-supported DOPC lipid bilayer (see QCM results, Figure 3D), while no adsorption could be observed outside of the GUV/GUV contact areas in the confocal images. This may partly be explained as a result of a more hydrophobic environment at the bilayer–bilayer contact area and thus an energetically driven phase separation within the confinement of two adjacent giant vesicles. The microgel particles, being more hydrophobic at higher temperature (40 °C), would assemble in the confinement between two adjacent GUVs due to the more hydrophobic environment compared to a single bilayer and their attractive interparticle interactions. Therefore, at 40 °C, the microgel particles can connect to the acyl chain region of two adjacent GUV bilayers and thus reduce the exposure of the hydrophobic regions. However, on the basis of our findings, further investigations which can correlate and increase the understanding of the local dynamics of the particles in the vicinity of the lipid bilayer, as well as the interactions between the two interfaces as a function of the particle conformation are still needed.

SUMMARY AND CONCLUSION

We present a straightforward method to generate giant unilamellar vesicles decorated with thermoresponsive soft cationic microgel particles that at low

temperatures significantly stabilize the GUVs. The microgel adsorption is reversible and can be triggered by the external parameter, temperature. Below the volume transition temperature T_{VPT}, the PNIPAM microgel particles behave as soft particles with a fuzzy surface as confirmed from the SAXS analysis. They adsorb on the GUV surfaces, forming densely packed 2D hexagonal arrays over the whole surface of each vesicle. Above their hydrophilic−hydrophobic transition, when the microgel particles become smaller, harder, and more hydrophobic, depleted zones coexist with domains of particles that are localized at the vesicle/vesicle interface. The microgel capability to adsorb to the GUV surface was found to be reduced as a consequence of the particle volume phase transition. Our data also suggest that the more hydrophobic character of the particles promotes penetration into the acyl region of the bilayer. The softness and deformability of the particles is crucial for the nature of the interaction between the particles and the model membrane.

The advantage of the proposed method is that it makes it possible to prepare large amounts of vesicles which are stabilized by particles. Here, the efficient stabilization of the microgel particles increases the lifetime of the vesicles, preventing fusion with neighboring vesicles over a broad range of temperatures. Thus, we envision that stimuli-responsive soft microgel particles that can vary their size, softness/deformability, and hydrophobicity on demand have great potential for future development of smart drug delivery systems and nanostructured materials. This approach could also be extended in the future to ellipsoidal-shaped thermosensitive microgel colloids with tailored aspect ratios[81] to investigate the combined effect of particle softness and shape anisotropy on the adhesive strength to lipid bilayers.

EXPERIMENTAL SECTION

Materials. 1,2-Dioleoyl-*sn*-glycero-3-phosphocholine (DOPC; M_w 786.11; $C_{44}H_{84}NO_8P$) and the fluorescent lipid probe, 1,2-dioleoyl-*sn*-glycero-3-phosphoethanolamine-*N*-(lissamine rhodamine B sulfonyl) (ammonium salt) (Liss Rhod PE; M_w 1301.72; $C_{68}H_{109}N_4O_{14}PS_2$), were purchased from Avanti Polar Lipids (Alabaster, AL, USA). Chloroform (purity ≥99.8%) was purchased from Sigma-Aldrich (Schnelldorf, Germany), and ethanol (purity 99.7%) was purchased from Solveco (Solveco AB, Rosenborg, Sweden). *N*-Isopropylmethacrylamide (NIPMAM; Aldrich), *N*,*N*′-methylenebisacrylamide (BIS; Fluka) monomers, and 2,2′-azobis(2-methylpropionamidine)dihydrochloride (V50; Fluka) were used as received. Water was purified using reverse osmosis (MilliRO; Millipore) and ion exchange (Milli-Q; Millipore).

Preparation of Thermoresponsive PNIPAM Microgel. In a typical procedure, NIPMAM (*N*-isopropylmethacrylamide; 2 g) as monomers, BIS (*N*,*N*′-methylenebisacrylamide; 0.136 g) as cross-linker, V50 (2,2′-azobis(2-methylpropionamidine)dihydrochloride; 0.01 g in 10 mL of water) as the initiator, and fluorescein-5-isothiocyanate (FITC) (2 mg dissolved in 87.8 mL of water) as the dye were polymerized by precipitation polymerization. The reaction was run at 80 °C for 4 h. The reaction mixture was passed through glass wool in order to remove particulate matter and further purified by three centrifugation cycles at 10 000 rpm for 20 min, with removal of the supernatant and redispersion between each cycle.

Preparation of Small Unilamellar Vesicles. Lipid vesicles were prepared by a modified version of the method of Barenholz *et al*.[82] Appropriate amounts of each lipid were weighted out and dissolved in chloroform. The chloroform was dried under nitrogen, followed by 12 h of removal of solvent traces under vacuum. The resultant dry lipid film was rehydrated with water to a concentration of 1 mg mL^{-1}, left above the melting point for 30 min, and then sonicated to a clear dispersion on ice (10 s on, 15 s off for 10 min). Titanium particles and large multilamellar liposomes and aggregates were removed by centrifugation for 10 min at 6000 rpm. The size of the vesicles in the supernatant was determined at a concentration of 100 μg mL^{-1} using dynamic light scattering (Nanosizer, Malvern) at an angle of 173° and a temperature of 25 °C.

Preparation of Giant Unilamellar Vesicles with PNIPAM Microgels. Giant unilamellar vesicles were prepared *in situ* on indium tin oxide (ITO)-coated microscope coverslips using the electroformation method.[79] Briefly, DOPC and the fluorescent membrane marker (0.5 mol % of Liss Rhod PE) were dissolved to 0.2 mg mL^{-1} in chloroform/methanol (2:1 volume ratio). Lipid solution (15 μL) was deposited onto the conductive side of the ITO-coated glass and allowed to dry. Subsequently, 10 μL of 1.4 wt % PNIPAM microgel dispersion was added onto the dried lipid film, and the entirety was sealed on a microscope slide. Conductive tape was then used to connect the ITO-coated coverslip to an electrode from the frequency generator. An AC field of 6 V operating at a frequency of 50 Hz was applied to the glass sandwich. GUV formation on the lipid-coated coverslip can be observed directly using confocal fluorescence microscopy.

Confocal Optical Microscopy. The confocal micrographs were monitored on a Leica SP5 confocal laser scanning microscope (CLSM) operated in the inverted mode (D6000I). The samples were contained between two ITO-coated cover glasses separated by a 100 μm spacer. A 488 nm Ar ion and a 543 nm HeNe laser were used to excite the red fluorescence of rhodamine B (543 nm) and the green fluorescence of fluorescein (488 nm), respectively. The samples were monitored *in situ* at different temperatures. The samples were heated from 20 to 40 °C and cooled again to 20 °C to check the reversibility.

Small Angle X-ray Scattering (SAXS). The scattering experiments were performed at the cSAXS beamline (X12SA at 11.2 keV photon energy, *i.e.*, a wavelength of $\lambda = 0.111$ nm) at the Swiss Light Source (Paul Scherrer Institut, Villigen, Switzerland). The 1 wt % PNIPAM microgel dispersions were measured in 1.0 mm quartz capillaries at 20 and 40 °C. The solvent was measured separately and subtracted from the data. Isotropic scattering data were obtained using standard procedures.

Dynamic (DLS) and Static Light Scattering (SLS). DLS and SLS were carried out on a 3D LSI spectrometer (LS Instruments, Switzerland) system equipped with a He−Ne laser ($\lambda = 633$ nm). The PNIPAM microgel dispersions were measured three times for 300 s duration at scattering angles from 45 to 135° with an increment of 15° at different temperatures. Temperature was varied from 20 to 55 °C in steps of 5 °C. Each samples was equilibrated for 30 min before recording scattered light. The resulting apparent hydrodynamic radius was calculated from a second-order cumulant analysis.

Zeta-Potential Measurements. The ζ-potential was estimated from the measurement of the particle electrophoretic mobility with a Zetasizer Nano-Z (Malvern Instruments Ltd., United Kingdom). Smoluchowski equation was used for converting the measured mobilities. The dispersions were highly diluted to avoid multiple-scattering effects.

Transmission Electron Microscopy (TEM). The TEM micrographs were obtained on a Philips CM100-Biotwin microscope operating at 80 kV. The samples were prepared by placing a 4 μL droplet of the 0.14 wt % PNIPAM microgel dispersion onto a 300 mesh carbon-coated copper grid.

Atomic Force Microscopy (SFM). SFM imaging was carried out using a Park atomic force microscope (XE 100 model, Park Systems) operated in tapping mode at room temperature. The samples were prepared by spin-coating the 0.14 wt % PNIPAM microgel dispersions onto freshly cleaned silicon wafers. Scan rates between 0.3 and 0.5 Hz were used.

Quartz Crystal Microbalance Measurements (QCM-D). A quartz crystal microbalance with dissipation (QCM-D) setup (Q Sense E4 system, Q Sense AB, Sweden) was used to measure the formation of phospholipid bilayers and the adsorption of microgel. The QCM-D sensors used in these experiments were quartz crystals connected to gold electrodes, coated with SiO_2, and having a fundamental frequency of 4.95 MHz (QSX 303, Q Sense). Changes in frequency and dissipation were recorded using Q-Soft software and analyzed using Q-Tools software, both from Q-sense (Q-sense AB, Sweden).

Formation of Supported Lipid Bilayers for the QCM-D Measurements. Supported lipid bilayers were formed on the SiO_2 surfaces *via* the vesicle fusion technique.[68] The SiO_2-coated sensors were soaked overnight in ethanol and then cleaned by soaking in 2 vol % of SDS for 1 h, followed by rinsing with copious amounts of ultrapure water and ethanol. The sensors were next dried under nitrogen and treated in a plasma cleaner (Harrick Scientific, USA) for 4 min. After plasma cleaning, the sensors were immediately inserted into the QCM-D cells. The temperature was set to the required value and allowed to equilibrate. Note that all solutions were maintained at the required temperature prior to introduction into the QCM cells using a peristaltic pump (IPC high precision multichannel dispenser, Ismatec, IDEX Health & Science, Germany), ensuring that no air bubbles were injected. The sensors were allowed to equilibrate in water until a stable baseline was reached. The dispersion of small unilamellar vesicles (100 μg mL^{-1}) was pumped onto each SiO_2 surface at a rate of 100 μL min^{-1}. After the completion of bilayer formation, recognized by a characteristic drop in frequency with a concomitant maximum increase in dissipation, the surface was rinsed with water to remove excess, unruptured vesicles.

Ellipsometry. Measurements were performed on a Rudolph thin film ellipsometer, type 436 (Rudolph Research, Fairfield, NJ), equipped with a xenon arc lamp and high-precision step motors, at a wavelength of 401.5 nm and an angle of incidence of 67.7°. Prior to the bilayer and microgel adsorption on a silica surface, four-zone measurements were performed in air and in water to determine the complex refractive index ($N = n - ik$) of the substrate bulk material as well as the refractive index (n_0) and thickness (d_0) of the outermost oxide layer. The samples were then injected into the cuvette, and the ellipsometric angles Ψ and Δ were recorded *in situ* every fifth second. If the optical properties of the substrate and the ambient media are known, the mean optical thickness (d_f) and refractive index (n_f) of the lipid and microgel layer can be solved numerically from the change in the optical angles Ψ and Δ. The measurement cell system, where the substrate surface is emerged vertically in a 5 mL thermostatted quartz cuvette, is a noncontinuous flow system with continuous stirring, giving the possibility to rinse the cuvette solution between additions. In a typical experiment, 500 μL of lipid stock solution was added to 4.5 mL water in the cuvette and the adsorption of the lipid was followed *in situ*. The liquid was then exchanged by pumping buffer into the cuvette at a flow rate of 12 mL/min for 5 min. Afterward, 50 μL of 1.4 wt % microgel stock solution was added and allowed to adsorb until reaching a plateau. This cycle was repeated at 25 and 40 °C. In these experiments, the formation of bilayer was always done at 25 °C, after which the temperature was increased to 40 °C. In order to accurately evaluate the film thickness of the absorbed microgel particles, we have first characterized the lipid bilayer at each temperature. On this basis, the microgel film thickness was determined from the measured ellipsometric response using a two-layer model that assumed an intact bilayer for the calculations.

The refractive index of the PNIPAM microgel particle at 401.5 nm was determined at 25 °C by using an Abbe 60 refractometer (Bellingham + Stanley Ltd., United Kingdom) in transmission mode. A concentration series from 0.137 to 1.37 wt % was measured at three different wavelengths of the emission line spectrum of the mercury lamp (453.8, 546.1, and 579 nm). A value of 1.601 was found at 401.5 nm from the extrapolation as function of λ with an empirical two-term Gauchy's equation: $n(\lambda) = A + B/\lambda^2$ (where $A = 1.49013$ and $B = 17846.86$ with λ given in nm).

Conflict of Interest: The authors declare no competing financial interest.

Acknowledgment. We gratefully acknowledge financial support from the Faculty of Science of Lund University, and the Swedish Research Council VR through the Linnaeus Center of Excellence on Organizing Molecular Matter. The Knut and Alice Wallenberg foundation funded the acquisition of the QCM-D instrument, the SFM and confocal microscope. SAXS experiments were performed at the cSAXS beam line (X12SA) of the Swiss Light Source at the Paul Scherrer Institute, Switzerland. We kindly acknowledge the expert help from our local contact Andreas Menzel. A.P.D. and T.N. acknowledge support from the Nanometer Structure Consortium (nmC@LU).

Supporting Information Available: Time-resolved bilayer formation probed by QCM-D at 20 °C (Figure S1). DOPC GUV formation in the presence of PNIPAM microgels under the influence of an alternating electric field at 20 °C. This material is available free of charge *via* the Internet at http://pubs.acs.org.

REFERENCES AND NOTES

1. Thiam, A. R.; Bremond, N.; Bibette, J. Adhesive Emulsion Bilayers under an Electric Field: From Unzipping to Fusion. *Phys. Rev. Lett.* **2011**, *107*, 068301(1)–068301(4).
2. Warshaviak, D. T.; Muellner, M. J.; Chachisvilis, M. Effect of Membrane Tension on the Electric Field and Dipole Potential of Lipid Bilayer Membrane. *Biochim. Biophys. Acta* **2011**, *1808*, 2608–2617.
3. Shimanouchi, T.; Sasaki, M.; Hiroiwa, A.; Yoshimoto, N.; Miyagawa, K.; Umakoshi, H.; Kuboi, R. Relationship between the Mobility of Phosphocholine Headgroups of Liposomes and the Hydrophobicity at the Membrane Interface: A Characterization with Spectrophotometric Measurements. *Colloids Surf., B* **2011**, *88*, 221–230.
4. Dimova, R.; Riske, K. A.; Aranda, S.; Bezlyepkina, N.; Knorr, R. L.; Lipowsky, R. Giant Vesicles in Electric Fields. *Soft Matter* **2007**, *3*, 817–827.
5. Riske, K. A.; Dimova, R. Electric Pulses Induce Cylindrical Deformations on Giant Vesicles in Salt Solutions. *Biophys. J.* **2006**, *91*, 1778–1786.
6. Aranda, S.; Riske, K. A.; Lipowsky, R.; Dimova, R. Morphological Transitions of Vesicles Induced by Alternating Electric Fields. *Biophys. J.* **2008**, *95*, L19–L21.
7. Sadik, M. M.; Li, J.; Shan, J. W.; Shreiber, D. I.; Lin, H. Vesicle Deformation and Poration under Strong DC Electric Fields. *Phys. Rev. E* **2011**, 83, 066316(1)–066316(9).
8. Herold, C.; Chwastek, G.; Schwille, P.; Petrov, E. P. Efficient Electroformation of Supergiant Unilamellar Vesicles Containing Cationic Lipids on ITO-Coated Electrodes. *Langmuir* **2012**, *28*, 5518–5521.
9. Mertins, O.; da Silveira, N. P.; Pohlmann, A. R.; Schröder, A. P.; Marques, C. M. Electroformation of Giant Vesicles from an Inverse Phase Precursor. *Biophys. J.* **2009**, *96*, 2719–2726.
10. Walde, P.; Consentino, K.; Engel, H.; Stano, P. Giant Vesicles: Preparations and Applications. *Chem. Biol. Chem.* **2010**, *11*, 848–865.
11. Needham, D.; Evans, E. Structure and Mechanical Properties of Giant Lipid (DMPC) Vesicle Bilayers from 20 °C below to 10 °C above the Liquid Crystal-Crystalline Phase Transition at 24 °C. *Biochemistry* **1988**, *27*, 8261–8269.
12. Dietrich, C.; Bagatolli, L. A.; Volovyk, Z. N.; Thomson, N. L.; Levi, M.; Jacobson, K.; Gratton, E. Lipid Rafts Reconstituted in Model Membranes. *Biophys. J.* **2001**, *80*, 1417–1428.
13. Ambroggio, E. E.; Separovic, F.; Bowie, J. H.; Fidelio, G. D.; Bagatolli, L. A. Direct Visualization of Membrane Leakage Induced by the Antibiotic Peptides: Maculatin, Citropin, and Aurein. *Biophys. J.* **2005**, *89*, 1874–1881.

14. Christensen, S. M.; Stamou, D. M. Sensing-Applications of Surface-Based Single Vesicle Arrays. *Sensors* **2010**, *10*, 11352–11368.
15. Chiu, D. T.; Wilson, C. F.; Ryttsén, F.; Strömberg, A.; Farre, C.; Karlsson, A.; Nordholm, S.; Gaggar, A.; Modi, B. P.; Moscho, A.; *et al.* Chemical Transformations in Individual Ultrasmall Biomimetic Containers. *Science* **1999**, *283*, 1892–1895.
16. Xu, T.; Zhang, N.; Nichols, H. L.; Shi, D.; Wen, X. Modification of Nanostructured Materials for Biomedical Applications. *Mater. Sci. Eng., C* **2007**, *27*, 579–594.
17. Quemeneur, F.; Rinaudo, M.; Maret, G.; Pépin-Donat, B. Decoration of Lipid Vesicles by Polyelectrolytes: Mechanism and Structure. *Soft Matter* **2010**, *6*, 4471–4481.
18. Ladavière, C.; Tribet, C.; Cribier, S. Lateral Organization of Lipid Membranes Induced by Amphiphilic Polymer Inclusions. *Langmuir* **2002**, *18*, 7320–7327.
19. Quemeneur, F.; Rinaudo, M.; Pépin-Donat, B. Influence of Molecular Weight and pH on Adsorption of Chitosan at the Surface of Large and Giant Vesicles. *Biomacromolecules* **2008**, *9*, 396–402.
20. Schulz, M.; Glatte, D.; Meister, A.; Scholtysek, P.; Kerth, A.; Blume, A.; Bacia, K.; Binder, W. H. Hybrid Lipid/Polymer Giant Unilamellar Vesicles: Effects of Incorporated Biocompatible PIB-PEO Block Copolymers on Vesicle Properties. *Soft Matter* **2011**, *7*, 8100–8110.
21. Shibayama, M.; Tanaka, T. Volume Phase Transition and Related Phenomena of Polymer Gels. *Adv. Polym. Sci.* **1993**, *109*, 1–62.
22. Lu, Y.; Ballauff, M. Thermoresponsive Core−Shell Microgels: From Colloidal Model Systems to Nanoreactors. *Prog. Polym. Sci.* **2011**, *36*, 767–792.
23. Hellweg, T. Responsive Core−Shell Microgels: Synthesis, Characterization, and Possible Applications. *J. Polym. Sci., Part B: Polym. Phys.* **2013**, *51*, 1073–1083.
24. Wu, J. Z.; Huang, G.; Hu, Z. B. Interparticle Potential and the Phase Behavior of Temperature-Sensitive Microgel Dispersions. *Macromolecules* **2003**, *36*, 440–448.
25. Rasmusson, M.; Routh, A.; Vincent, B. Flocculation of Microgel Particles with Sodium Chloride and Sodium Polystyrene Sulfonate as a Function of Temperature. *Langmuir* **2004**, *20*, 3536–3542.
26. Zaccone, A.; Crassous, J. J.; Béri, B.; Ballauff, M. Quantifying the Reversible Association of Thermosensitive Nanoparticles. *Phys. Rev. Lett.* **2011**, *107*, 168303(1)–168303(4).
27. McParlane, J.; Dupin, D.; Saunders, J. M.; Lally, S.; Armes, S. P.; Saunders, B. R. Dual pH-Triggered Physical Gels Prepared from Mixed Dispersions of Oppositely Charged pH-Responsive Microgels. *Soft Matter* **2012**, *8*, 6239–6247.
28. Crassous, J. J.; Millard, P. E.; Mihut, A. M.; Polzer, F.; Ballauff, M.; Schurtenberger, P. Asymetric Self-Assembly of Oppositely Charged Composite Microgels and Gold Nanoparticles. *Soft Matter* **2012**, *8*, 1648–1656.
29. Brugger, B.; Rütten, S.; Phan, K.-H.; Möller, M.; Richtering, W. The Colloidal Suprastructure of Smart Microgels at Oil−Water Interfaces. *Angew. Chem., Int. Ed.* **2009**, *48*, 3978–3981.
30. Schmidt, S.; Liu, T.; Rütten, S.; Phan, K.-H.; Möller, M.; Richtering, W. Influence of Microgel Architecture and Oil Polarity on Stabilization of Emulsions by Stimuli-Sensitive Core−Shell Poly(*N*-isopropylacrylamide-*co*-methacrylic acid) Microgels: Mickering *versus* Pickering Behavior? *Langmuir* **2011**, *27*, 9801–9806.
31. Richtering, W. Responsive Emulsions Stabilized by Stimuli-Sensitive Microgels: Emulsions with Special Non-Pickering Properties. *Langmuir* **2012**, *28*, 17218–17229.
32. Geisel, K.; Isa, L.; Richtering, W. Unraveling the 3D Localization and Deformation of Responsive Microgels at Oil/Water Interfaces: A Step Forward in Understanding Soft Emulsion Stabilizers. *Langmuir* **2012**, *28*, 15770–15776.
33. Destribats, M.; Lapeyre, V.; Wolfs, M.; Sellier, E.; Leal-Calderon, F.; Ravaine, V.; Schmitt, V. Soft Microgels as Pickering Emulsion Stabilisers: Role of Particle Deformability. *Soft Matter* **2011**, *7*, 7689–7698.
34. Destribats, M.; Lapeyre, V.; Sellier, E.; Leal-Calderon, F.; Ravaine, V.; Schmitt, V. Origin and Control of Adhesion between Emulsion Drops Stabilized by Thermally Sensitive Soft Colloidal Particles. *Langmuir* **2012**, *28*, 3744–3755.
35. Gautier, F.; Destribats, M.; Perrier-Cornet, R.; Dechézelles, J.-F.; Giermanska, J.; Héroguez, V.; Ravaine, S.; Leal-Calderon, F.; Schmitt, V. Pickering Emulsions with Stimulable Particles: From Highly- to Weakly-Covered Interfaces. *Phys. Chem. Chem. Phys.* **2007**, *9*, 6455–6462.
36. Saleem, Q.; Liu, B.; Gradinaru, C. C.; Macdonald, P. M. Lipogels: Single-Lipid-Bilayer-Enclosed Hydrogel Spheres. *Biomacromolecules* **2011**, *12*, 2364–2374.
37. Kiser, P. F.; Wilson, G.; Needham, D. A Synthetic Mimic of the Secretory Granule for Drug Delivery. *Nature* **1998**, *394*, 459–462.
38. Kiser, P. F.; Wilson, G.; Needham, D. Lipid-Coated Microgels for the Triggered Release of Doxorubicin. *J. Controlled Release* **2000**, *68*, 9–22.
39. Stauch, O.; Uhlmann, T.; Fröhlich, M.; Thomann, R.; El-Badry, M.; Kim, Y.-K.; Schubert, R. Mimicking a Cytoskeleton by Coupling Poly(*N*-isopropylacrylamide) to the Inner Leaflet of Liposomal Membranes: Effects of Photopolymerization on Vesicle Shape and Polymer Architecture. *Biomacromolecules* **2002**, *3*, 324–332.
40. Markström, M.; Gunnarsson, A.; Orwar, O.; Jesorka, A. Dynamic Microcompartmentalization of Giant Unilamellar Vesicles by Sol−Gel Transition and Temperature Induced Shrinking/Swelling of Poly(*N*-isopropyl acrylamide). *Soft Matter* **2007**, *3*, 587–595.
41. Jesorka, A.; Markström, M.; Orwar, O. Controlling the Internal Structure of Giant Unilamellar Vesicles by Means of Reversible Temperature Dependent Sol−Gel Transition of Internalized Poly(*N*-isopropylacrylamide). *Langmuir* **2005**, *21*, 1230–1237.
42. Campillo, C.; Pépin-Donat, B.; Viallat, A. Responsive Viscoelastic Giant Lipid Vesicles Filled with a Poly(*N*-isopropylacrylamide) Artificial Cytoskeleton. *Soft Matter* **2007**, *3*, 1421–1427.
43. Faivre, M.; Campillo, C.; Viallat, A.; Pepin-Donat, B. Responsive Giant Vesicles Filled with Poly(*N*-isopropylacrylamide) Sols or Gels. *Prog. Colloid Polym. Sci.* **2006**, *133*, 41–44.
44. Schmidt, S.; Zeiser, M.; Hellweg, T.; Duschl, C.; Fery, A.; Möhwald, H. Adhesion and Mechanical Properties of PNIPAM Microgel Films and Their Potential Use as Switchable Cell Culture Substrates. *Adv. Funct. Mater.* **2010**, *20*, 3235–3243.
45. Mukherjee, S.; Ghosh, R. N.; Maxfield, F. R. Endocytosis. *Physiol. Rev.* **1997**, *77*, 759–803.
46. Conner, S. D.; Schmid, S. L. Regulated Portals of Entry into the Cell. *Nature* **2003**, *422*, 37–44.
47. Smith, A. E.; Helenius, A. How Viruses Enter Animal Cells. *Science* **2004**, *304*, 237–242.
48. Rejman, J.; Oberle, V.; Zuhorn, I. S.; Hoekstra, D. Size-Dependent Internalization of Particles *via* the Pathways of Clathrin- and Caveolae-Mediated Endocytosis. *Biochem. J.* **2004**, *377*, 159–169.
49. Monticelli, L.; Salonen, E.; Ke, P. C.; Vattulainen, I. Effects of Carbon Nanoparticles on Lipid Membranes: A Molecular Simulation Perspective. *Soft Matter* **2009**, *5*, 4433–4445.
50. da Rocha, E. L.; Caramori, G. F.; Rambo, C. R. Nanoparticle Translocation through a Lipid Bilayer Tuned by Surface Chemistry. *Phys. Chem. Chem. Phys.* **2013**, *15*, 2282–2290.
51. Wong-Ekkabut, J.; Baoukina, S.; Triampo, W.; Tang, I.-M.; Tieleman, P.; Monticelli, L. Computer Simulation Study of Fullerene Tanslocation through Lipid Membranes. *Nat. Nanotechnol.* **2008**, *3*, 363–368.
52. Champion, J. A.; Mitragotri, S. Role of Target Geometry in Phagocytosis. *Proc. Natl. Acad. Sci. U.S.A.* **2006**, *103*, 4930–4934.
53. Decuzzi, P.; Ferrari, M. The Adhesive Strength of Non-spherical Particles Mediated by Specific Interactions. *Biomaterials* **2006**, *27*, 5307–5314.
54. Decuzzi, P.; Ferrari, M. The Receptor-Mediated Endocytosis of Nonspherical Particles. *Biophys. J.* **2008**, *94*, 3790–3797.
55. Yang, K.; Ma, Y. Q. Computer Simulation of the Translocation of Nanoparticles with Different Shapes Across a Lipid Bilayer. *Nat. Nanotechnol.* **2010**, *5*, 579–583.

56. Tao, L.; Hu, W.; Liu, Y.; Huang, G.; Sumer, B. D.; Gao, J. Shape-Specific Polymeric Nanomedicine: Emerging Opportunities and Challenges. *Exp. Biol. Med.* **2011**, *236*, 20–29.
57. Shah, S.; Liu, Y.; Hu, W.; Gao, J. Modeling Particle Shape-Dependent Dynamics in Nanomedicine. *J. Nanosci. Nanotechnol.* **2011**, *11*, 919–928.
58. Liu, Y.; Tan, J.; Thomas, A.; Ou-Yang, D.; Muzykantov, V. R. The Shape of Things To Come: Importance of Design in Nanotechnology for Drug Delivery. *Therapeutic Delivery* **2012**, *3*, 181–194.
59. Ding, H. M.; Tian, W. D.; Ma, Y. Q. Designing Nanoparticle Translocation through Membranes by Computer Simulations. *ACS Nano* **2012**, *6*, 1230–1238.
60. Dasgupta, S.; Auth, T.; Gompper, G. Wrapping of Ellipsoidal Nano-particles by Fluid Membranes. *Soft Matter* **2013**, *9*, 5473–5482.
61. Helwa, Y.; Dave, N.; Liu, J. Electrostatically Directed Liposome Adsorption, Internalization and Fusion on Hydrogel Microparticles. *Soft Matter* **2013**, *9*, 6151–6158.
62. Geest, B. G. D.; Stubbe, B. G.; Jonas, A. M.; Thienen, T. V.; Hinrichs, W. L. J.; Demeester, J.; Smedt, S. C. D. Self-Exploding Lipid-Coated Microgels. *Biomacromolecules* **2006**, *7*, 373–379.
63. Schmidt, S.; Motschmann, H.; Hellweg, T.; von Klitzing, R. Thermoresponsive Surfaces by Spin-Coating of PNIPAM-*co*-PAA Microgels: A Combined AFM and Ellipsometry Study. *Polymer* **2008**, *49*, 749–756.
64. Lopez-Leon, T.; Ortega-Vinuesa, J. L.; Bastos-Gonzalez, D.; Elaïssari, A. Cationic and Anionic Poly(*N*-isopropylacrylamide) Based Submicron Gel Particles: Electrokinetic Properties and Colloidal Stability. *J. Phys. Chem. B* **2006**, *110*, 4629–4636.
65. Stieger, M.; Pedersen, J. S.; Lindner, P.; Richtering, W. Are Thermoresponsive Microgels Model Systems for Concentrated Colloidal Suspensions? A Rheology and Small-Angle Neutron Scattering Study. *Langmuir* **2004**, *20*, 7283–7292.
66. Wu, X.; Pelton, R. H.; Hamielec, A. E.; Woods, D. R.; McPhee, W. The Kinetics of Poly(*N*-isopropylacrylamide) Microgel Latex Formation. *Colloid Polym. Sci.* **1994**, *272*, 467–477.
67. Sierra-Martin, B.; Choi, Y.; Romero-Cano, M. S.; Cosgrove, T.; Vincent, B.; Fernandez-Barbero, A. Microscopic Signature of a Microgel Volume Phase Transition. *Macromolecules* **2005**, *38*, 10782–10787.
68. McConnel, H.; Watts, T.; Weis, R.; Brian, A. Supported Planar Membranes in Studies of Cell–Cell Recognition in the Immune System. *Biochim. Biophys. Acta* **1986**, *864*, 95–106.
69. Höök, F.; Kasemo, B.; Nylander, T.; Fant, C.; Sott, K.; Elwing, H. Variations in Coupled Water, Viscoelastic Properties, and Film Thickness of a Mefp-1 Protein Film during Adsorption and Cross-Linking: A Quartz Crystal Microbalance with Dissipation Monitoring, Ellipsometry, and Surface Plasmon Resonance Study. *Anal. Chem.* **2001**, *73*, 5796–5804.
70. Reimhult, E.; Höök, F.; Kasemo, B. Vesicle Adsorption on SiO_2 and TiO_2: Dependence on Vesicle Size. *J. Chem. Phys.* **2002**, *117*, 7401–7404.
71. Pan, J.; Tristram-Nagle, S.; Kučerka, N.; Nagle, J. F. Temperature Dependence of Structure, Bending Rigidity, and Bilayer Interactions of Dioleoylphosphatidylcholine Bilayers. *Biophys. J.* **2008**, *94*, 117–124.
72. Wiener, M.; White, S. Structure of a Fluid Dioleoylphosphatidylcholine Bilayer Determined by Joint Refinement of X-ray and Neutron Diffraction Data. II. Distribution and Packing of Terminal Methyl Groups. *Biophys. J.* **1992**, *61*, 428–433.
73. Pomorska, A.; Shchukin, D.; Hammond, R.; Cooper, M. A.; Grundmeier, G.; Johannsmann, D. Positive Frequency Shifts Observed upon Adsorbing Micron-Sized Solid Objects to a Quartz Crystal Microbalance from the Liquid Phase. *Anal. Chem.* **2010**, *82*, 2237–2242.
74. Vaughan, R. D.; O'Sullivan, C. K.; Guillbault, G. G. Development of a Quartz Crystal Microbalance (QCM) Immunosensor for the Detection of Listeria Monocytogenes. *Enzyme Microb. Technol.* **2001**, *29*, 635–638.
75. Le, D. T.; Zanna, S.; Frateur, I.; Marcus, P.; Loubiŕe, P.; Dague, E.; Mercier-Bonin, M. Real-Time Investigation of the Muco-Adhesive Properties of *Lactococcus lactis* Using a Quartz Crystal Microbalance with Dissipation Monitoring. *Biofouling* **2012**, *28*, 479–490.
76. Fatisson, J.; Domingos, R. F.; Wilkinson, K. J.; Tufenkji, N. Deposition of TiO_2 Nanoparticles onto Silica Measured Using a Quartz Crystal Microbalance with Dissipation Monitoring. *Langmuir* **2009**, *25*, 6062–6069.
77. Reviakine, I.; Johannsmann, D.; Richter, R. P. Hearing What You Cannot See and Visualizing What You Hear: Interpreting Quartz Crystal Microbalance Data from Solvated Interfaces. *Anal. Chem.* **2011**, *83*, 8838–8848.
78. Johannsmann, D.; Reviakine, I.; Richter, R. P. Dissipation in Films of Adsorbed Nanospheres Studied by Quartz Crystal Microbalance (QCM). *Anal. Chem.* **2009**, *81*, 8167–8176.
79. Angelova, M. I.; Dimitrov, D. Liposome Electroformation. *Faraday Discuss. Chem. Soc.* **1986**, *81*, 303–311.
80. Wu, J.; Zhou, B.; Hu, Z. Phase Behavior of Thermally Responsive Microgel Colloids. *Phys. Rev. Lett.* **2003**, *90*, 048304(1)–048304(4).
81. Crassous, J. J.; Dietsch, H.; Pfleiderer, P.; Malik, V.; Diaz, A.; Hirshi, L. A.; Drechsler, M.; Schurtenberger, P. Preparation and Characterization of Ellipsoidal-Shaped Thermosensitive Microgel Colloids with Tailored Aspect Ratios. *Soft Matter* **2012**, *8*, 3538–3548.
82. Barenholz, Y.; Gibbes, D.; Litman, B.; Goll, J.; Thompson, T.; Carlson, F. A Simple Method for the Preparation of Homogeneous Phospholipid Vesicles. *Biochemistry* **1977**, *16*, 2806–2810.